



Article

Assessing Snow Water Retrievals over Ocean from Coincident Spaceborne Radar Measurements

Mengtao Yin * and Cheng Yuan

Emergency Management College, Nanjing University of Information Science & Technology,
Nanjing 210044, China

* Correspondence: 003093@nuist.edu.cn

Abstract: Spaceborne snow water retrievals over oceans are assessed using a multiyear coincident dataset of CloudSat Cloud Profiling Radar (CPR) and Global Precipitation Mission (GPM) Dual-frequency Precipitation Radar (DPR). Various factors contributing to differences in snow water retrievals between CPR and DPR are carefully considered. A set of relationships between radar reflectivity (Z_e) and snow water content (SWC) at Ku- and W-bands is developed using the same microphysical assumptions. It is found that surface snow water contents from CPR are much larger than those from DPR at latitudes above 60° , while surface snow water contents from DPR slightly exceed those from CPR at latitudes below 50° . Coincident snow water content profiles between CPR and DPR are further divided into two conditions. One is that only CPR detects the falling snow. Another is that both CPR and DPR detect the falling snow. The results indicate that about 88% of all snow water content profiles are under the first condition and usually associated with light snowfall events. The remaining snow water content profiles are generally associated with moderate and heavy snowfall events. Moreover, CPR surface snow water contents are larger than DPR ones at high latitudes because most light snowfall events are misdetected by DPR due to its low sensitivity. DPR surface snow water contents exceed CPR ones at low latitudes because CPR may experience a significant reduction in backscattering efficiency of large particles and attenuation in heavy snowfall events. The low sensitivity of DPR also causes a noticeable decrease in detected snow layer depth. The results presented here can help in developing global snowfall retrieval algorithms using multi-radars.



Citation: Yin, M.; Yuan, C. Assessing Snow Water Retrievals over Ocean from Coincident Spaceborne Radar Measurements. *Remote Sens.* **2023**, *15*, 1140. <https://doi.org/10.3390/rs15041140>

Academic Editor: Joan Bech

Received: 20 January 2023

Revised: 13 February 2023

Accepted: 18 February 2023

Published: 19 February 2023



Copyright: © 2023 by the authors. Licensee MDPI, Basel, Switzerland. This article is an open access article distributed under the terms and conditions of the Creative Commons Attribution (CC BY) license (<https://creativecommons.org/licenses/by/4.0/>).

Keywords: GPM; CloudSat; radar; snow; retrieval

1. Introduction

Snowfall, as a major form of precipitation at mid and high latitudes, can significantly affect the global hydrological cycle and energy budget. Over land, the falling snow can remain on the ground for several days and strongly alter the surface albedo [1]. Over oceans, the falling snow is related to the complex interaction with the ocean surface, since it can cool and refresh the ocean surface through melting. [2]. The falling snow on the ground is also an important freshwater resource, especially over the mountainous regions [3]. The demand to accurately quantify global snowfall intensities has been increased dramatically from scientific and social fields for better understanding of the global hydrological cycle and monitoring of the global water resource. While ground-based observations are available for snowfall detection over land, spaceborne observation are vital for detecting the falling snow over oceans [4,5]. Compared with satellite rainfall retrievals, which have a long history, satellite snowfall retrievals are still under development. Early studies mainly employed satellite passive microwave sensors for snowfall detection [2,6]. Their results have demonstrated the potential of high-frequency microwave channels in retrieving snowfall intensities. Satellite active microwave sensors were not available until the launch of CloudSat [7], which carried the first spaceborne microwave radar, Cloud Profiling Radar

(CPR) [8]. Recently, the Global Precipitation Measurement (GPM) mission [5,9] further emphasized the importance of global snowfall detection using satellite active and passive microwave sensors. Its carried sensors, including GPM Microwave Imager (GMI) [10] and Dual-frequency Precipitation Radar (DPR) [11], can substantially improve the quantitative estimates of global snowfall events.

Currently, the CloudSat CPR and the GPM satellite sensors are primarily employed for global snowfall retrievals. The CloudSat CPR is a nadir-looking microwave radar at the W-band (94 GHz). Benefiting from its high sensitivity and horizontal spatial resolution, CPR is found to perform well in detecting light snowfall events globally. CloudSat snowfall retrievals have been compared with several independent ground-based measurements [12–14] and commonly used in global and regional snowfall studies. Liu [15] employed CPR observations to characterize global snow clouds. Palerme et al. [16] derived the climatological Antarctic precipitation characteristics using CloudSat products. Kulie et al. [17] as well as Kulie and Milani [18] explored shallow cumuliform snowfall events using multiyear CloudSat CPR observations. Milani et al. [19] evaluated CloudSat snowfall estimates and presented a multiyear snowfall climatology in the region south of 60°S. The GPM DPR is a dual-frequency radar consisting of 13.6 (Ku-band) and 35.5 (Ka-band) GHz. Unlike CloudSat CPR, the DPR is a cross-track instrument, implying that its swath width is much larger than that of CPR. Due to its relatively low sensitivity and horizontal spatial resolution, DPR is more suitable for moderate and heavy snowfall events. Adhikari et al. [20] used three-year GPM DPR Ku-band measurements to characterize global snow precipitation features and properties. Subsequently, Adhikari and Liu [21] explored global distributions of thundersnow events from six-year GPM DPR Ku-band measurements. More recently, Chase et al. [22,23] examined current GPM DPR snowfall retrieval microphysical assumptions and presented a new DPR retrieval algorithm of snow particle-size distribution parameters. The GMI is a conical microwave imager with high-frequency channels at fine horizontal spatial resolutions. The official Goddard profiling algorithm (GPROF) [24] has provided falling snow estimates. Panegrossi et al. [25] explored the sensitivity of GMI high-frequency channels to falling snow at high latitudes. Yin and Liu [26] proposed a variational snowfall retrieval algorithm for GMI. In addition, Rysman et al. [27,28] presented an all-surface snowfall retrieval algorithm for GMI. Nevertheless, current GMI snowfall retrieval algorithms heavily rely on initial snowfall profiles derived from CPR or DPR measurements, further highlighting the significance of spaceborne microwave radars in global snowfall retrievals.

Since CloudSat CPR and GPM DPR provide valuable global snowfall measurements, it is important to compare and assess their snowfall retrievals for future improvements on global snowfall estimates. Tang et al. [29] directly compared CPR and DPR precipitation retrieval products. Their results indicated that CPR outperforms DPR in terms of light snowfall detection. On the other hand, DPR seems to observe more snowfall events than CPR at low and mid latitudes, possibly due to different scanning characteristics and precipitation phase classification methods between CPR and DPR. Casella et al. [30] evaluated GPM DPR snowfall detection capability through comparisons with CloudSat CPR. It is seen that DPR retrieval products miss a large portion of light snowfall events, while CPR retrieval products underestimate intense snowfall events. The misdetection of snowfall events by DPR is mainly caused by its large minimum detectable reflectivity values. The side lobe clutter mitigation method also removes some weak snowfall signals associated with small radar reflectivity values around minimum detectable reflectivities. In addition, they pointed out that different precipitation phase classification methods used between CPR and DPR retrieval products can further complicate the direct comparison of their snowfall retrievals. Skofronick-Jackson et al. [31] compared GPM and CloudSat snowfall products for a multiyear period. In general, DPR fails to detect most light snowfall events, while CPR underestimates heavy snowfall rates due to decreased backscattering efficiency of large particles and hydrometeor attenuation at W-band, which is also mentioned by some recent studies [32,33]. They deliberately explored different factors contributing to CPR and DPR

retrieval product discrepancies, including surface precipitation phase classification method, instrument sampling (orbits and spatial resolutions), instrument sensitivity (minimum detectable reflectivities) and retrieval algorithm assumptions (reflectivity to snowfall rate relationships). After mitigating these four issues, the underestimation of global snowfall rates by DPR is reduced to under 20%.

In this study, spaceborne radar snowfall estimates from multiyear coincident CloudSat CPR and GPM DPR measurements [34] are assessed. Instead of directly using radar products, snow water content profiles are firstly derived from CPR and DPR reflectivity profiles using the same microphysical assumptions. Besides snowfall rate, snow water content is also provided by CloudSat and GPM precipitation products. One advantage of deriving snow water content is that there is no need to assume particle fall velocity models which also contribute to precipitation product discrepancies. Only CPR and DPR measurements over oceans are included for this study, since ground-based observations for directly evaluating satellite snowfall retrievals are lacking. Other factors contributing to snowfall retrieval discrepancies highlighted by Skofronick-Jackson et al. [31] are also carefully considered and mitigated for a more equitable comparison. This study aims to explain the remaining snowfall retrieval differences between CPR and DPR after mitigation steps, which is important for truly assessing the snowfall detection capabilities of current spaceborne radars. The results presented in this study can help develop global snowfall retrieval algorithms for the upcoming Aerosol Cloud Convection and Precipitation (ACCP) mission [35,36] with available Ku-, Ka- and W-band spaceborne radar measurements.

The remaining of this paper is organized as follows. Section 2 describes data sources, mitigation methods to reduce snow water retrieval differences and retrieval methods. Section 3 presents the assessment of CPR and DPR snow water retrievals and discusses the remaining retrieval differences between CPR and DPR. Section 4 gives a summary and conclusions for this study.

2. Data Sources and Methods

2.1. Satellite Sensor Description

The CloudSat–GPM coincidence dataset [34] is employed for multiyear assessment of snow water retrievals. It mainly consists of collocated radar reflectivity profiles between CPR and DPR as well as ancillary European Centre for Medium-range Weather Forecasts (ECMWF) state variables interpolated to CPR bins. It is easy to incorporate other parameters from CPR and DPR standard products using collocation indices. CloudSat 2B-GEOPROF, GPM 2A Radar and GPM 2B Combined products are also used for constructing oceanic annual mean surface snow water content maps.

The CloudSat was launched into a sun-synchronous orbit. The CPR operates at the 94 GHz (W-band) with nearly global coverage. Its footprint size is about 2.3 km along the track and 1.4 km across the track. Its vertical bin size is about 240 m. The GPM Core Observatory was launched into a non-sun-synchronous orbit at 65° of inclination. The DPR operates at 13.6 (Ku-band) and 35.5 (Ka-band) GHz with a spatial coverage between 65°S and 65°N. The DPR Ku-band has one scanning pattern of normal scan (NS), while the DPR Ka-band has two scanning patterns of match scan (MS) and high-sensitivity scan (HS). The Ku NS has 49 footprints. In the Ka MS, there are 25 footprints matched to the central footprints of Ku NS from 13 to 37. It has a footprint size of about 5.2 km at nadir and 5.6 km at the largest scan angle. The vertical bin size of DPR is about 125 m for Ku NS and Ka MS. While different orbits between CloudSat and GPM satellites can cause differences in instrument sampling between CPR and DPR, the use of coincident CPR and DPR measurements automatically ensures the same spatial coverage of spaceborne radars between 65°S and 65°N. Different spatial resolutions between CPR and DPR are also considered. Since the footprint size of CPR (about 2 km) is smaller than that of DPR (about 5 km), the beam averaging method is applied to CPR reflectivity profiles. A CPR profile matched to a single DPR profile is composited by averaging all CPR profiles within a searching radius of 4 km around the location of that DPR profile. The vertical bin size

of CPR (about 240 m) is larger than that of DPR Ku NS and Ka MS (about 125 m). In the original coincidence dataset, a single CPR bin is matched with the first DPR bin above this CPR bin searching from the bottom of a matched DPR profile. Vertically averaging two nearest DPR bins above and below a CPR bin has been tested, producing very similar results to the original dataset. Accordingly, the vertical matching method is kept the same for this coincidence dataset.

2.2. Data Limitations and Processing Methods

As mentioned by Skofronick-Jackson et al. [31], different surface precipitation phase classification methods can significantly affect snowfall retrievals especially over oceans where temperature lapse rates near the surface can be steep. At high latitudes, the low-level temperature inversion is frequently observed and can directly modify the surface precipitation phase [37]. Any surface precipitation phase classification method not including the information of temperature structure near the surface may overestimate the occurrence of surface snowfall events. Therefore, a parameterization of surface snowfall probability from Sims and Liu [38] is adopted here to select radar profiles associated with surface-falling snow. This parameterization has included the information of the near-surface air temperature and low-level vertical temperature lapse rate calculated from ECMWF ancillary state variables for CPR to distinguish solid and liquid precipitation. A radar profile with a surface snowfall probability higher than 50% is selected for this study.

Discrepancies in instrument characteristics between CPR and DPR can cause noticeable differences in snowfall retrievals. In terms of instrument sensitivity, the minimum detectable reflectivity of CPR is around -30 dBZ [8]. The precipitation threshold of CPR reflectivity is defined as -15 dBZ [39,40]. On the other hand, Hamada and Takayabu [41] showed that the post-launch minimum detectable reflectivity of the DPR Ku-band is about 12 dBZ over oceans, beyond the design specification [5]. Skofronick-Jackson et al. [31] also showed this minimum detectable reflectivity value of 12 dBZ for the DPR Ku-band. In this study, the minimum detectable reflectivity of CPR and DPR is defined as -30 and 12 dBZ, respectively. The precipitation threshold of -15 dBZ is adopted for CPR. Besides, the employment of different radar frequencies between CPR and DPR also contributes to differences in snowfall retrievals. As mentioned by previous studies [31,33], the backscattering of large snow particles at the W-band can become non-Rayleigh, leading to differences in backscattering efficiency of snow particles between CPR and DPR. The attenuation at different radar frequencies is another issue to be considered. At the W-band, the gaseous attenuation is mainly due to water vapor, which is not negligible at low latitudes [7]. The attenuation due to frozen hydrometeors can be substantial in heavy snowfall events, partially balanced by multiple scattering [42]. Nevertheless, the uncertainty in modeling the effect of multiple scattering in heavy snowfall events remains large. Supercooled liquid water may also attenuate W-band radar reflectivities significantly. The CPR is not designed to detect cloud liquid water droplets. One approach for correcting this type of attenuation is to use coincident cloud liquid water retrievals from GPM precipitation products [43], while this approach may contain some unavoidable errors. At the Ku-band, the attenuation effect on radar reflectivity is generally negligible regardless of water vapor, frozen hydrometeors and supercooled liquid water in snowfall events [44,45]. It is seen that the estimation of attenuation due to hydrometeors and multiple scattering at the W-band may produce some biases. Therefore, only gaseous attenuation at the W-band provided by CloudSat 2B-GEOPROF product is corrected for CPR.

Different scanning patterns between CPR and DPR are finally considered. Since the DPR is a cross-track instrument, its surface clutter layer varies from 0.5 to 2 km over oceans. Skofronick-Jackson et al. [31] only used the near-nadir beams of DPR for reducing the height of surface clutter layer. In this study, 49 beams of DPR Ku NS are employed. Hereafter, DPR refers to the DPR Ku-band. The impact of increased surface clutter layer height on snow water retrievals will be evaluated later. The information of lowest clutter free bin for DPR is provided by the DPR 2A Radar product. The CPR is a nadir-pointing

instrument with a nearly constant surface clutter layer height over oceans. The lowest 1 km layer above the surface is treated as the surface clutter layer for CPR. The near-surface bin is defined as the first bin above the surface clutter layer for CPR and DPR. Eventually, about 19,100 coincident radar profiles with CPR reflectivity in the near-surface bin exceeding -15 dBZ were selected for this study. It is worth mentioning that only about 40 coincident radar profiles were found under the circumstance that DPR detects surface-falling snow and CPR fails to detect it, possibly due to the remaining mismatch errors between CPR and DPR. The geolocations of selected coincident radar profiles are displayed in Figure 1. The color scheme from Green [46] is employed. Most radar profiles for surface snowfall events are located at latitudes above 50° . The locations of radar profiles are distributed more homogeneously in the southern hemisphere. The time span of selected radar profiles covers from March 2014 to October 2017.

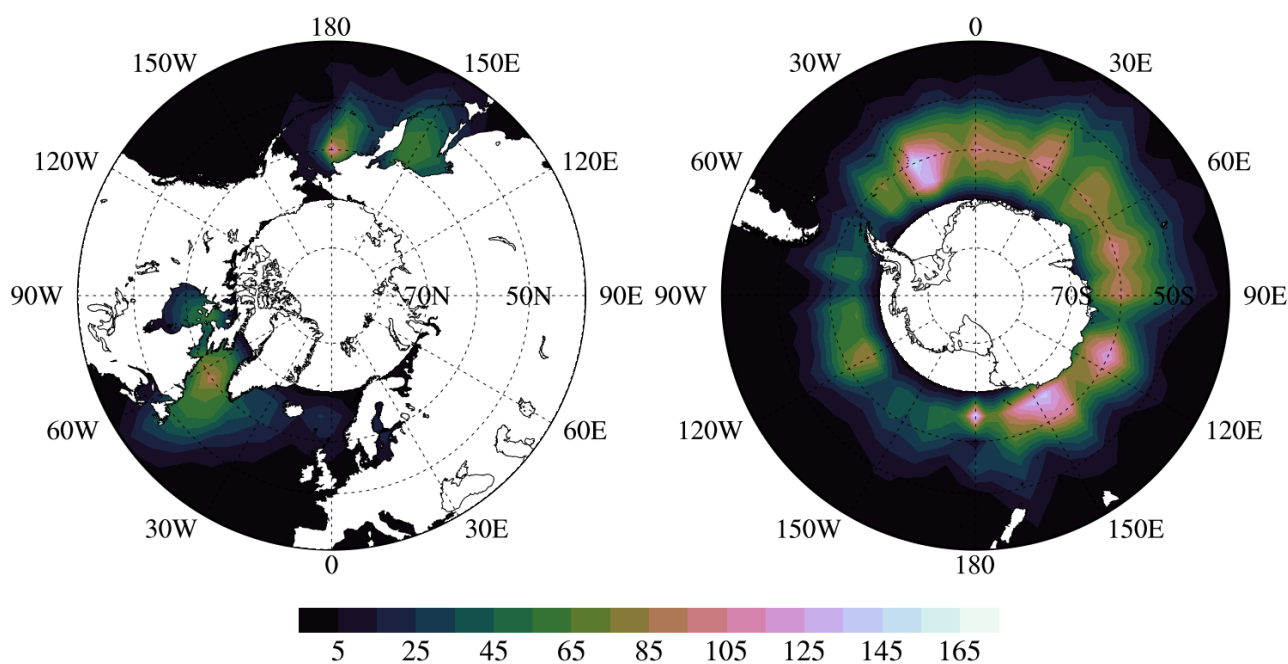


Figure 1. Geolocations of coincident radar profiles for surface snowfall events within $5^\circ \times 5^\circ$ boxes.

2.3. Snow Water Retrieval Methods

Snowfall retrieval algorithms of CPR and DPR precipitation products employ different microphysical assumptions, resulting in different implicit relationships between snowfall rate/snow water content and radar reflectivity. In the CloudSat 2C-SNOW-PROFILE product, pristine models for small particles and aggregate models for large particles are used for calculating the backscattering properties of snow particles [47]. The snow particle-size distribution is assumed in the exponential form. The slope and intercept parameters of particle-size distribution are retrieved using an optimal estimation method [48]. This optimal method minimizes a cost function representing the weighted sum of differences between simulated and observed radar reflectivities as well as differences between a priori and estimated snow microphysical properties. Snowfall rate or snow water contents profiles are derived from retrieved particle-size distribution parameter profiles. In the GPM 2A Radar product, snow particles are modeled as spherical particles [49]. The snow particle-size distribution is assumed as Gamma distribution where the shape factor is assumed to be known and constant. The slope and intercept parameters are constrained by a relationship between snowfall rate and mass-weighted mean diameter. This relationship between snowfall rate and mass-weighted mean diameter is modified to minimize the difference between estimated and calculated path-integrated attenuation and increase the consistency with Ka-band reflectivity. The GPM 2B Combined product also provides snowfall estimates for DPR Ku NS [50]. It assumes a normalized gamma distribution of snow particle size and

employs nonspherical pristine and aggregate models [51]. DPR Ku-band reflectivities are used to derive initial precipitation estimates. The snow particle-size distribution parameters are updated to be consistent with path-integrated attenuation, DPR Ka-band reflectivity and GMI brightness temperature. As shown by Skofronick-Jackson et al. [31], snowfall retrievals from GPM 2B Combined product are close to those from the GPM 2A DPR NS product, since the GPM 2B Combined product also mainly relies on DPR Ku-band reflectivity.

For eliminating the impact of underlying microphysical assumptions on snow water retrievals, a set of relationships between radar reflectivity (Z_e) and snow water content (SWC) at W and Ku-band is developed using the same microphysical assumptions. Sector and dendrite models from Liu [52] are selected for representing small snow particles. The sector particle is composed of three identical ellipsoids sharing the same center, while the dendrite particle has many branches extending from the particle center. Both are commonly observed in nature. One oblate aggregate model from Honeyager et al. [53] is selected for representing snow aggregates. The oblate aggregate has an irregular shape and is constructed from tiny rosette particles. The maximum particle size for sector and dendrite models is restricted by 8 mm, while that for the oblate aggregate model can reach about 11 mm. The backscattering cross sections of the three snow particle models are calculated using discrete dipole approximation (DDA) [54]. The exponential form of snow particle-size distribution is assumed as

$$N(D) = N_0 \exp(-\Lambda D) \quad (1)$$

where D is the snow particle size, N_0 is the intercept parameter, and Λ is the slope parameter. The exponential behavior of snow particle-size distribution has been found under different atmospheric conditions from previous snowfall studies using airborne measurements [55–57]. Forty-nine pairs of N_0 and Λ provided by in situ measurements of Braham [55] are adopted for developing Z_e -SWC relationships. After obtaining the snow particle-size distribution, Z_e and SWC can be computed from the following equations

$$Z_e = \frac{\lambda^4}{\pi^5 |K|^2} \int_{D_{\min}}^{D_{\max}} N(D) \sigma_{\text{bsc}}(D) dD \quad (2)$$

and

$$\text{SWC} = \int_{D_{\min}}^{D_{\max}} N(D) m(D) dD \quad (3)$$

where λ is the wavelength, K is a function of the dielectric constant of water, D_{\max} and D_{\min} are upper and lower limits of snow particle size, $N(D)$ is the particle-size distribution, $\sigma_{\text{bsc}}(D)$ is the backscattering cross section of snow particle, and $m(D)$ is the snow particle mass. Figure 2 shows derived Z_e -SWC relationships for CPR and DPR using sector, dendrite and oblate aggregate models. Red and blue lines are obtained by least-square fitting of all data points and can be represented by the following equations

$$\text{SWC} = 0.024 Z_e^{0.75} \text{ (CPR)} \quad (4)$$

$$\text{SWC} = 0.013 Z_e^{0.56} \text{ (DPR)} \quad (5)$$

where SWC is in g m^{-3} and Z_e is in $\text{mm}^6 \text{ m}^{-3}$. It is worth noting that either explicit or implicit Z_e -SWC relationship is very sensitive to employed microphysical assumptions. The root-mean-square difference of the natural logarithm of snow water content ($\ln\text{SWC}$) between data points and fitting lines in Figure 2 is about 0.43 and 0.56 for W and Ku-band, respectively. Since $d\ln\text{SWC} = dS/S$, it means that the relative error of fitting lines due to the spreading of data points is about 50%, consistent with results from Liu [15]. As mentioned by previous studies [44,45], the uncertainty in the single-frequency Z_e -SWC relationship is generally large due to variability in snowflake microphysics. There is no intention to derive the best Z_e -SWC relationships at different radar frequencies for snowfall retrieval

algorithms. A set of Z_e -SWC relationships derived above is only a tool to make a more equitable comparison between CPR and DPR.

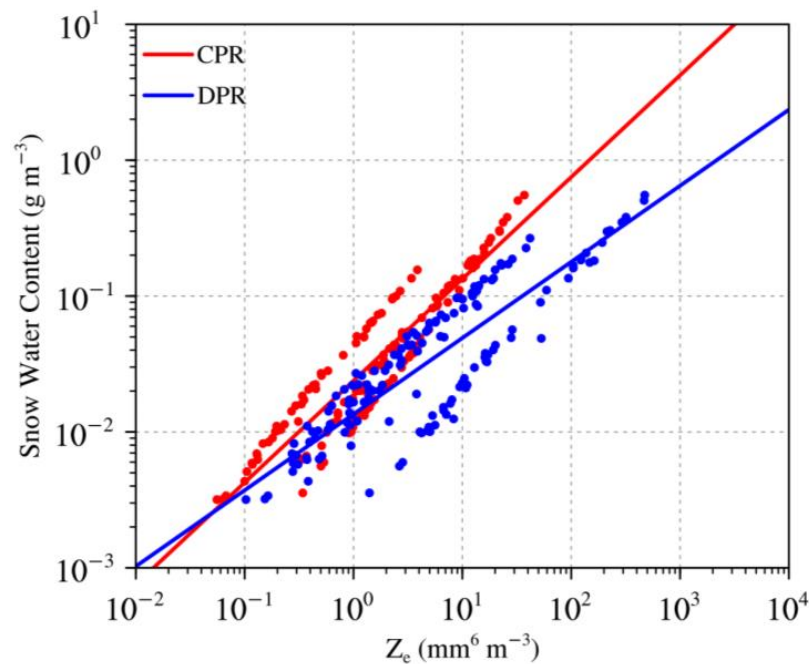


Figure 2. Z_e -SWC relationships for CPR and DPR using sector, dendrite and oblate aggregate models.

3. Assessment of Spaceborne Radar Snow Water Retrievals

3.1. Satellite Annual Mean Surface Snow Water Distributions

The annual mean surface snow water content distributions over oceans for the one year of 2016 are firstly derived from CPR and DPR radar reflectivities as well as the GPM 2B Combined product to demonstrate the effect of instrument sensitivity and retrieval methods on snow water retrievals. The spatial coverage of snow water retrievals is restricted to latitudes between 65°S and 65°N for reducing instrument sampling differences. The same parameterization of the surface snowfall probability from Sims and Liu [38] is used to classify the surface precipitation phase. CPR and DPR radar reflectivity is obtained from CloudSat 2B-GEOPROF and GPM 2A Radar product, respectively. Snow water content profiles are converted from CPR and DPR reflectivity profiles using Z_e -SWC relationships (4) and (5). The GPM 2B Combined product directly provides snow water content profiles for DPR Ku NS. Figures 3 and 4 present annual mean surface snow water retrievals over oceans from CPR and DPR reflectivities as well as the GPM 2B Combined product. Surface snow water contents from the GPM 2B Combined product are much smaller than those from DPR in both hemispheres. It implies that the underestimation of surface snow water content by the GPM 2B Combined product is caused by employed retrieval methods. On the other hand, surface snow water contents from CPR are much larger than those from DPR at latitudes above 60° , especially over the southern hemisphere. Since the same retrieval method is applied to CPR and DPR, differences in surface snow water contents between CPR and DPR are likely due to their different minimum detectable reflectivities, as mentioned in Section 2.

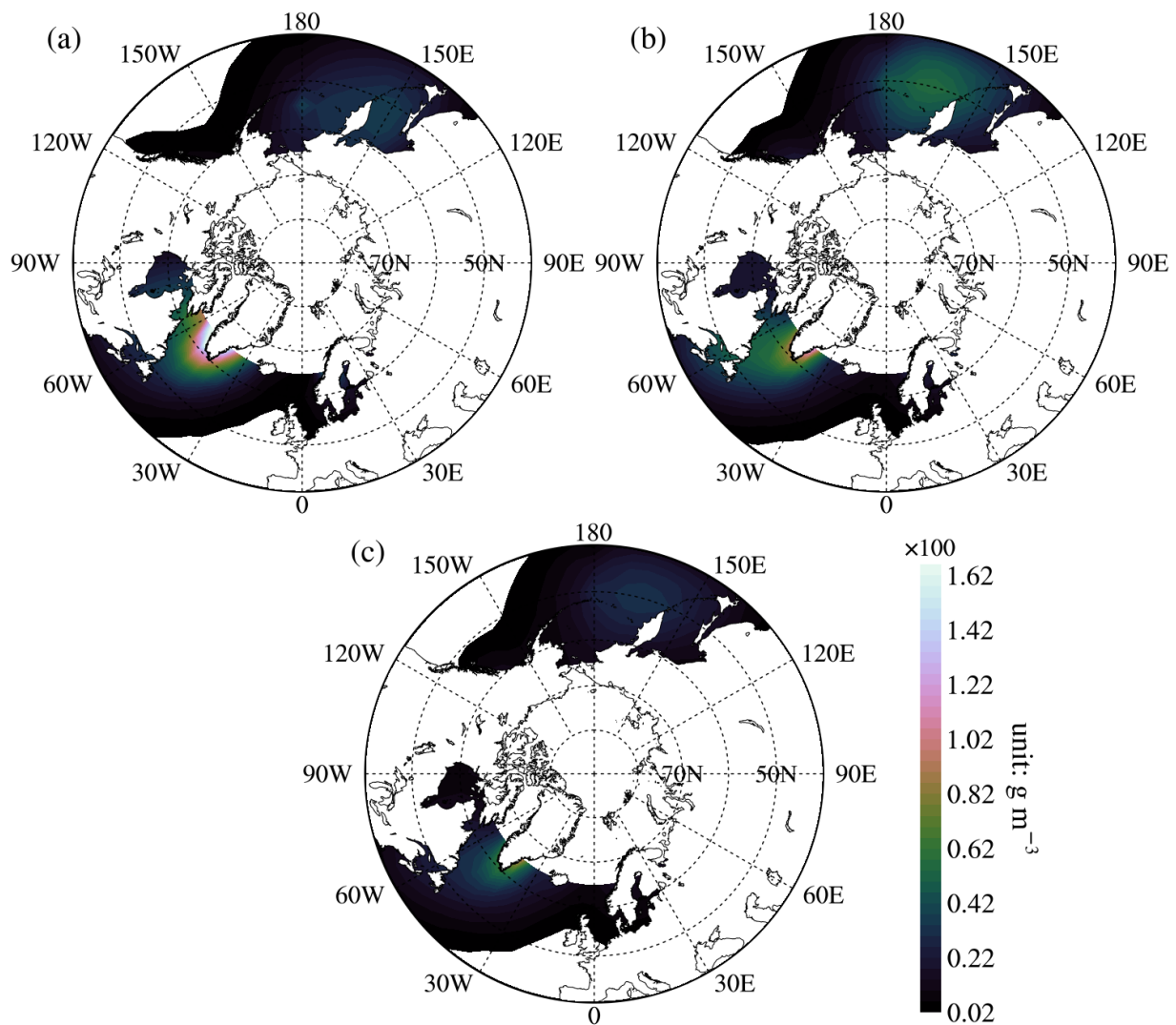


Figure 3. Northern hemisphere annual mean surface snow water content distributions over oceans for the one year of 2016 derived from (a) CPR reflectivities, (b) DPR reflectivities and (c) the GPM 2B combined product. Results are multiplied by 100.

It can be seen in Figures 3 and 4 that surface snow water contents from DPR exceed those from CPR over broad regions at lower latitudes. To fully explore this finding, differences in annual mean surface snow water content distributions over oceans between CPR and DPR (CPR minus DPR) are presented in Figure 5. In the northern hemisphere, there is a region between 30°W and 60°W where positive differences can reach above 12 mg m^{-3} at latitudes above 60°N, while negative differences between 150°E and 180°E can be as large as -3 mg m^{-3} at latitudes below 50°N. In southern hemisphere, there is a broad region at latitudes above 60°S where positive differences are generally large and can reach up to 8 mg m^{-3} . At latitudes below 50°S, most regions are associated with negative differences smaller than -1 mg m^{-3} . Overall, surface snow water retrievals from CPR are much larger than those from DPR for most regions at latitudes above 60°. At latitudes below 50°, surface snow water retrievals from DPR become larger than those from CPR over a broad region with small differences, especially over the southern hemisphere. In the following part, the multiyear coincident spaceborne radar measurements are employed to further explore snow water retrievals from CPR and DPR.

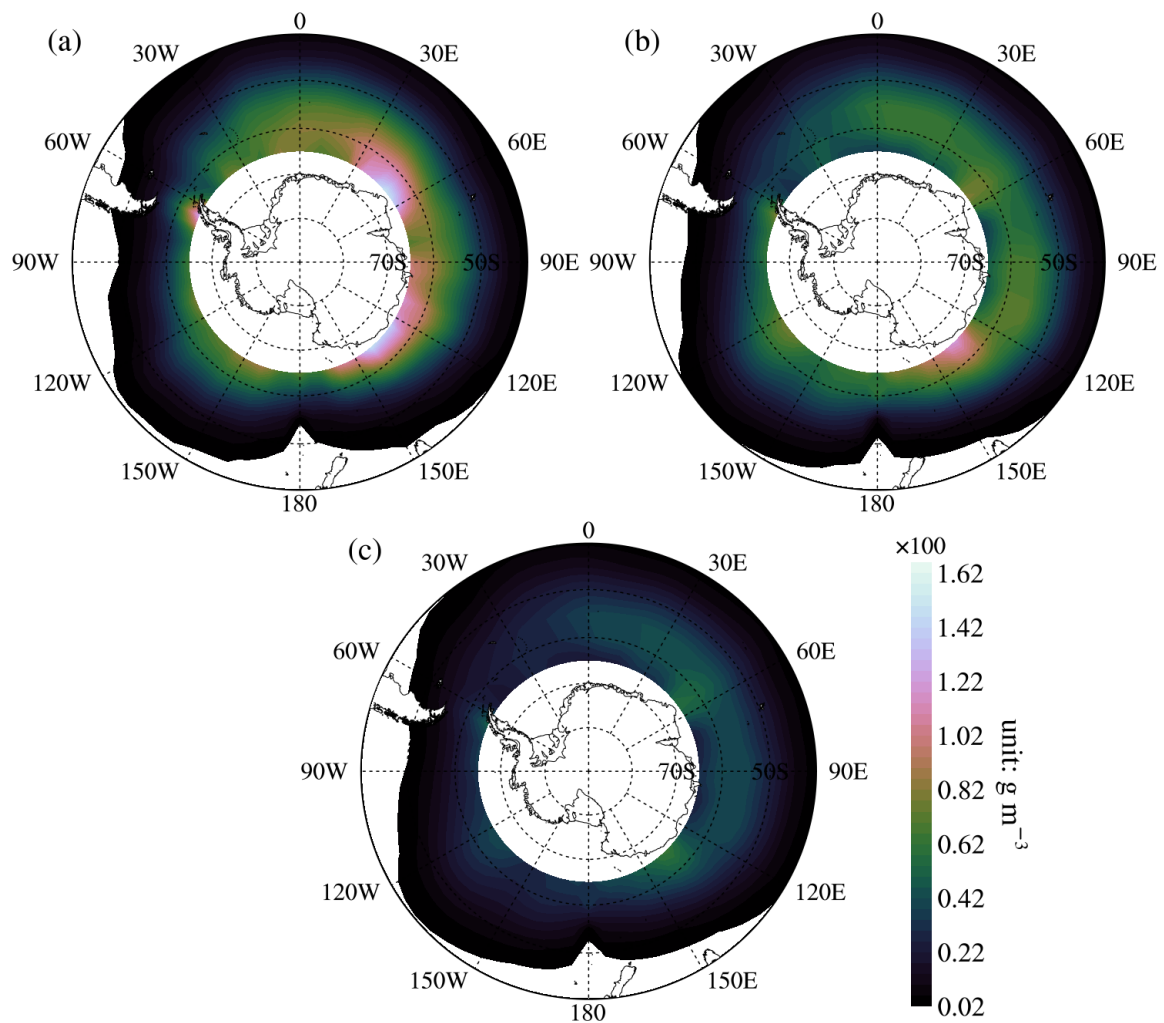


Figure 4. Same as Figure 3 except for southern hemisphere.

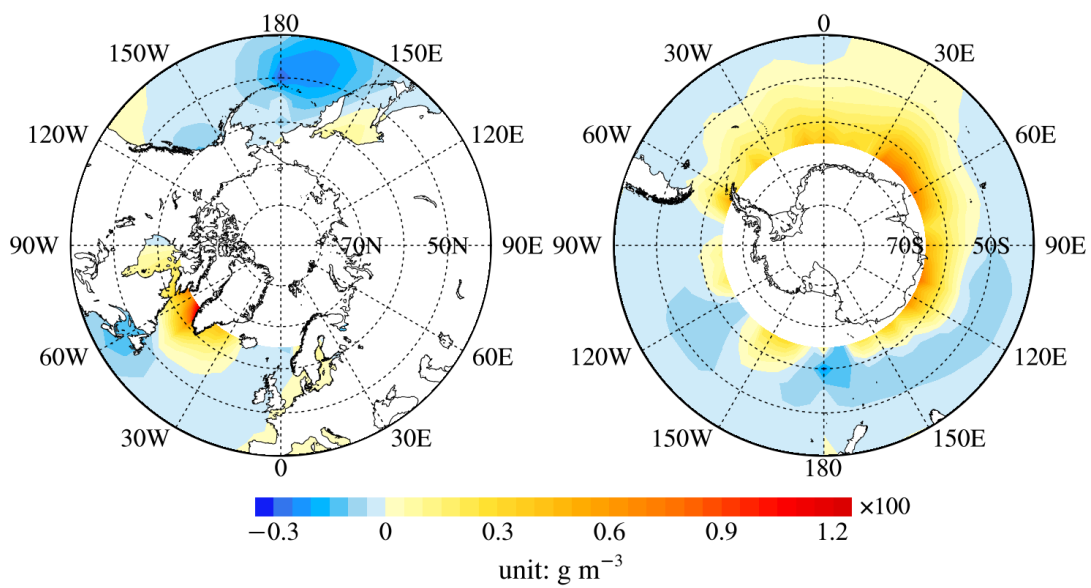


Figure 5. Differences in annual mean surface snow water content distributions over oceans for the one year of 2016 between CPR and DPR (CPR minus DPR).

3.2. Snow Water Retrievals from Coincident Satellite Radars

It is important to examine whether surface snow water retrievals from multiyear coincident CPR and DPR measurements mimic their annual mean surface snow water retrievals over oceans. The period of coincident CPR and DPR measurements covers from March 2014 to October 2017. Zonally mean surface snow water contents from coincident CPR and DPR measurements over oceans are displayed in Figure 6. For reasonable sampling numbers, 10° latitude band is used for producing mean surface snow water content values. All snowfall events occur at latitudes above 40° . It is clearly seen that mean surface snow water contents from DPR generally increase towards lower latitudes, while those from CPR tend to have larger values at higher latitudes. In the northern hemisphere, mean surface snow water contents from CPR are larger than those from DPR with differences decreasing towards lower latitudes. In the southern hemisphere, mean surface snow water contents from DPR are smaller than those from CPR at latitudes above 50°S . Only between 40°S and 50°S , mean surface snow water contents from DPR slightly exceed those from CPR. It is evident that surface snow water retrievals from coincident CPR and DPR measurements capture the main features of their annual mean surface snow water retrievals over oceans.

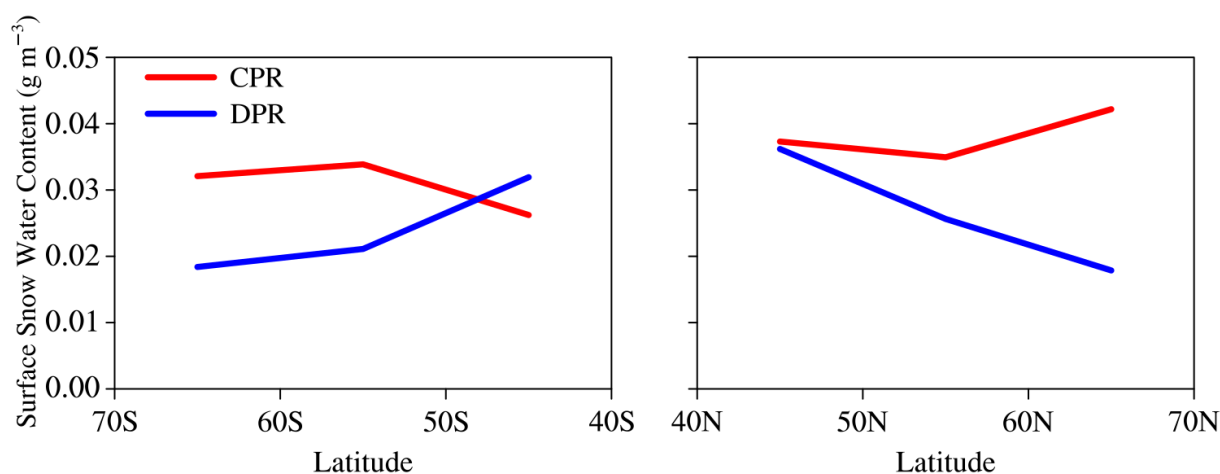


Figure 6. Zonally mean surface snow water contents for CPR and DPR in 10° latitude band over oceans.

Next, snow water content profiles derived from coincident CPR and DPR measurements are divided into two conditions for better assessment. The snow water path is firstly defined as the integrated snow water content in the vertical column. It is worth noting that the CPR snow water path is always larger than zero because CPR reflectivities in near-surface bins of selected radar profiles need to exceed the precipitation threshold of -15 dBZ. One condition is that the DPR snow water path is equal to zero, meaning that only CPR detects the falling snow. The other condition is that the DPR snow water path is larger than zero, meaning that both CPR and DPR detect the falling snow. There are about 16,800 snow water content profiles under the first condition, taking up about 88% of all snow water content profiles. It implies that DPR only detects about 12% of CPR snowfall events, generally consistent with the statistics from Skofronick-Jackson et al. [31]. This discrepancy in snowfall detection is mainly due to different instrument sensitivity between CPR and DPR. The DPR minimum detectable reflectivity of 12 dBZ over oceans tend to exclude most light snowfall events. All snow water content profiles under the first condition are further grouped based on their CPR snow water paths at an interval of 100 g m^{-2} . Data count and surface snow contribution of each group is presented in Figure 7. More than 12,000 snow water content profiles are associated with CPR snow water paths smaller than 100 g m^{-2} . Even though this group only contains snow water profiles associated with very light snowfall events, it can still contribute more than 20% to total surface snow water content of all CPR snow water content profiles due to its large

data count. Data count and surface snow contributions of each group are then dramatically decreased with increasing CPR snow water paths. When the CPR snow water path is larger than 300 g m^{-2} , the data count of each group is smaller than 500, and its surface snow contribution is smaller than 10%. Nevertheless, the remaining groups of snow water content profiles can contribute 48% to total CPR surface snow water content.

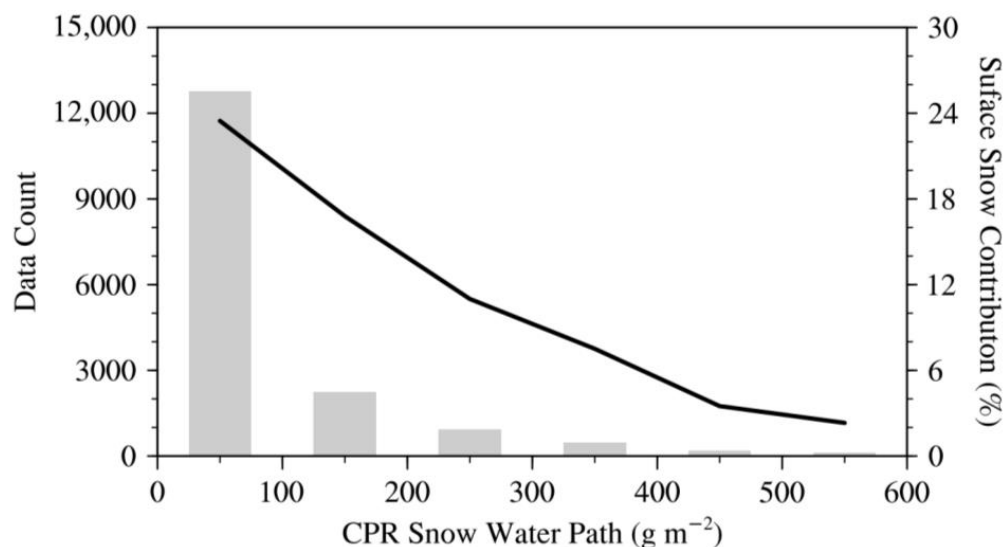


Figure 7. Data count (bar) and surface snow contribution (line) of snow water content profiles grouped by CPR snow water paths under the condition that only CPR detects the falling snow.

There are only about 2300 snow water content profiles under the second condition that both CPR and DPR detect the falling snow. CPR and DPR snow water content profiles are also grouped based on DPR snow water paths at an interval of 100 g m^{-2} . Since snow water content profiles are associated with moderate and heavy snowfall events under this condition, CPR measurements tend to contain some biases. Therefore, the DPR snow water path is employed to group snow water content profiles. Figure 8 shows the mean surface snow water content and data count of each group for CPR and DPR. From the second group with DPR snow water paths larger than 100 g m^{-2} , surface snow water contents from DPR exceed those from CPR. Differences in surface snow water contents between CPR and DPR increase with increasing DPR snow water paths. When DPR snow water paths are larger than 700 g m^{-2} , the DPR surface snow water content is about 0.29 g m^{-3} , while the CPR surface snow water content can only reach about 0.1 g m^{-3} . As mentioned before, CPR is not suitable for heavy snowfall events due to its decreased backscattering efficiency of large particles and significant hydrometeor attenuation. On the other hand, when DPR snow water paths are smaller than 200 g m^{-2} , a large portion of snowfall events are not detected by DPR. After that, the number of DPR snow water content profiles without surface snow water contents is decreased dramatically. At small DPR snow water paths, snow clouds may produce light solid precipitation near the surface, possibly misdetected by DPR. Besides, CPR may also partly overestimate surface-falling snow due to its surface clutter.

To directly compare the snowfall detection capability between CPR and DPR, occurrence frequencies of CPR and DPR surface snow water contents are displayed in Figure 9a. It is clearly seen that DPR is not able to measure surface snow water contents smaller than 0.05 g m^{-3} due to its large minimum detectable reflectivity. The peak of occurrence frequencies of CPR surface snow water contents is about 16% at 0.07 g m^{-3} . After that, the occurrence frequencies decrease quickly with increasing CPR surface snow water contents, implying that CPR performs poorly in detecting moderate and heavy snowfall events. When CPR surface snow water contents are larger than 0.21 g m^{-3} , the corresponding occurrence frequencies are smaller than 1%. In contrast, the peak of occurrence frequencies of DPR surface snow water contents is located at 0.11 g m^{-3} with a value of about 13%. The

occurrence frequencies remain above 5% until DPR surface snow water contents increase above 0.25 g m^{-3} , indicating that DPR is suitable for detecting heavy snowfall events. In Figure 9b, the impact of DPR surface clutter layer height on snow water retrievals is explored. The subset refers to the central beams of DPR Ku NS (20 to 28) with low surface clutter layer heights. Differences in occurrence frequencies of CPR and DPR surface snow water contents between DPR full scan and its subset are comparably small. At small surface snow water contents, differences in occurrence frequencies of CPR and DPR surface snow water contents are confined to 2%. When CPR and DPR surface snow water contents increase, differences in occurrence frequencies generally decrease. Since the surface clutter layer for CPR is the constant 1 km layer, it implies that the impact of DPR surface clutter layer height on snow water retrievals is not evident.

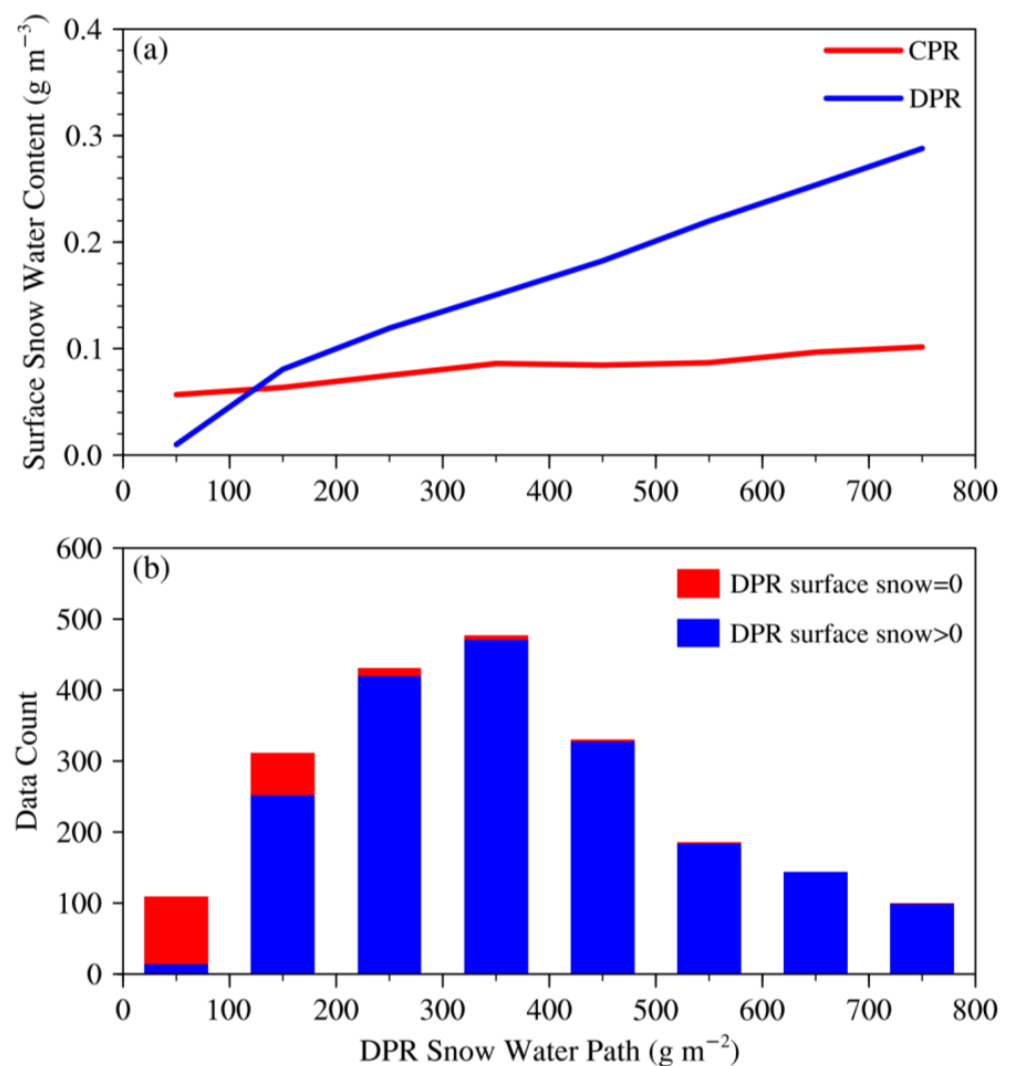


Figure 8. (a) Mean surface snow water content and (b) data count of CPR and DPR snow water content profiles grouped by DPR snow water paths under the condition that both CPR and DPR detect the falling snow.

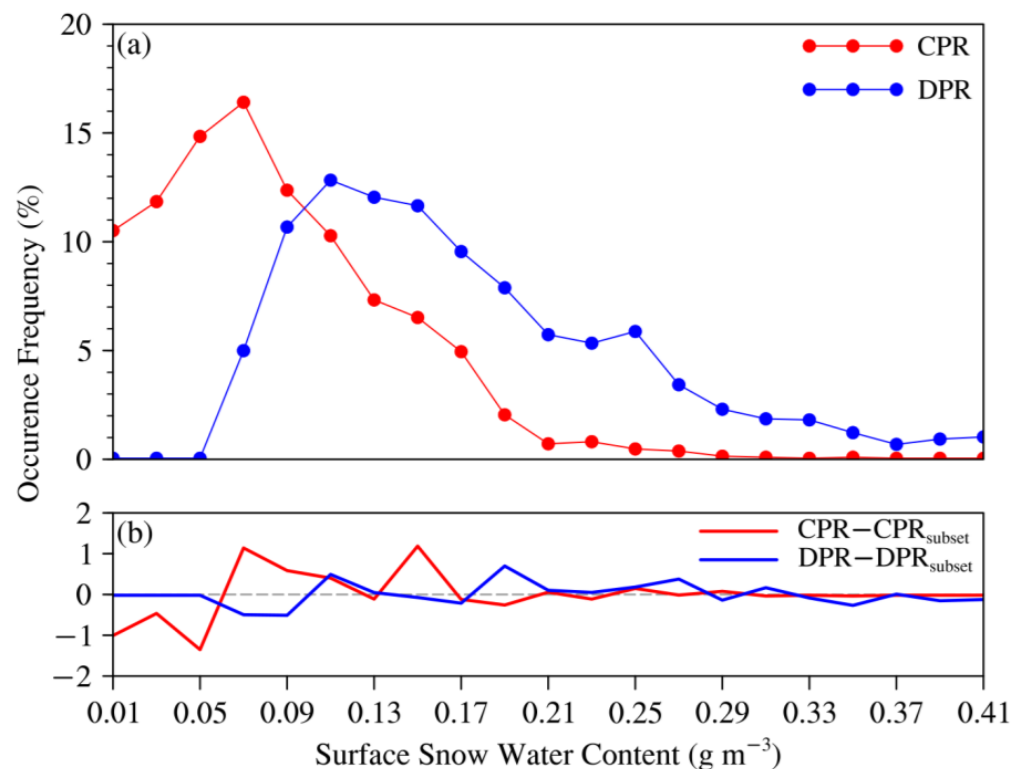


Figure 9. (a) Occurrence frequencies of CPR and DPR surface snow water contents as well as (b) differences in occurrence frequencies between DPR full scan and its central beams under the condition that both CPR and DPR detect the falling snow.

From the analysis above, it seems that DPR underestimates surface snow water contents for small snow water paths, while CPR underestimates surface snow water contents for large snow water paths. Consequently, zonally mean CPR and DPR snow water paths and their occurrence frequencies under the second condition that both CPR and DPR detect the falling snow are shown in Figure 10. DPR mean snow water paths are larger than CPR ones in both hemispheres. In the northern hemisphere, CPR and DPR mean snow water paths increase towards lower latitudes. In the southern hemisphere, DPR mean snow water paths increase with decreasing latitudes, while CPR mean snow water paths gradually decrease towards lower latitudes. Since CPR snow water paths may contain large biases in moderate and heavy snowfall events, DPR snow water paths can better characterize snowfall events under this condition. It seems that heavy snowfall events are more frequent at lower latitudes, which is physically reasonable because convective clouds that likely produce more intense falling snow are more frequently formed at lower latitudes. Moreover, the difference in mean snow water paths between CPR and DPR reaches its maximum value at latitudes below 50° in both hemispheres, implying that CPR is subject to more hydrometeor attenuation and reduction in backscattering efficiency of large particles at lower latitudes. On the other hand, occurrence frequencies of snow water paths are generally small in a range from 9% to 16%, since a large amount of snow water content profiles only detected by CPR exist in each 10° latitude band and can substantially contribute to surface snow water contents. Therefore, mean surface water contents from CPR are much larger than those from DPR at latitudes above 60° , likely due to snow water content profiles associated with light snowfall events misdetected by DPR, while mean surface water contents from DPR exceed those from CPR at latitudes below 50° likely due to snow water content profiles associated with heavy snowfall events underestimated by CPR.

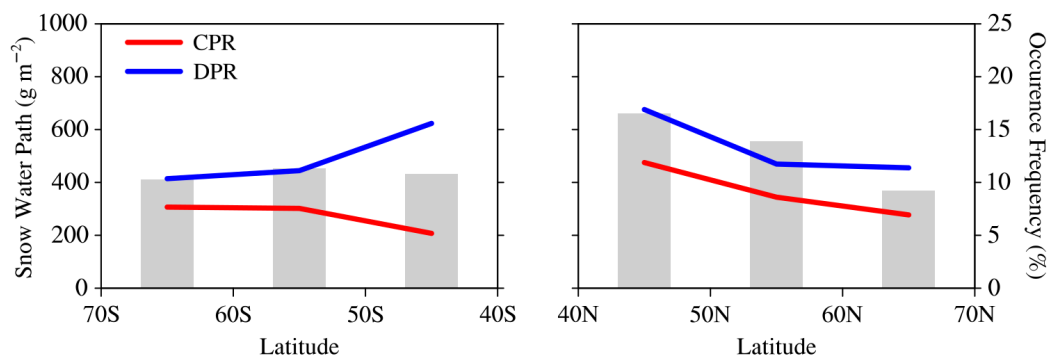


Figure 10. Zonally mean snow water paths (line) and their occurrence frequencies (bar) for CPR and DPR in 10° latitude band over oceans under the condition that both CPR and DPR detect the falling snow.

Besides surface snow water content, we explored vertical profiles of snow water content for CPR and DPR. Figure 11 presents CPR and DPR mean snow water content profiles over oceans. Snow water contents in the surface clutter layer are copied from those of the near-surface bin. CPR snow layers generally extend to about 6 km above the ground regardless of DPR snow water paths, while DPR snow layers become deeper with increasing DPR snow water paths and can only extend to about 4 km. At large DPR snow water paths, CPR snow water content profiles may contain negative biases, leading to decreased snow layer depths. On the other hand, most falling snow at high altitudes is light and not detected by DPR. Therefore, DPR snow water depths are significantly restricted by its low sensitivity. In addition, DPR snow water content profiles tend to have a different vertical structure compared with CPR ones for group 1. DPR snow water contents near the surface are extremely small, while CPR ones can still reach above 0.05 g m^{-3} . This discrepancy in snow water contents near the surface between CPR and DPR for group 1 is also likely caused by DPR large minimum detectable reflectivity. When snow clouds in group 1 produce light solid precipitation near the surface, DPR is not able to detect most of them near the surface.

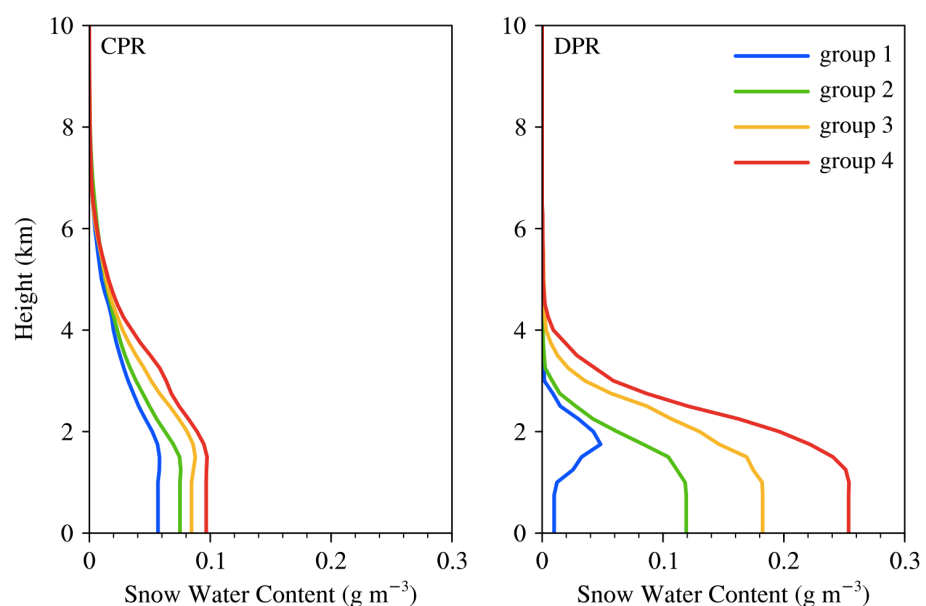


Figure 11. CPR and DPR mean snow water content profiles over oceans. Group 1 to 4 corresponds to DPR snow water path interval between 0 and 100 g m^{-2} , 200 and 300 g m^{-2} , 400 and 500 g m^{-2} , 600 and 700 g m^{-2} .

4. Conclusions

In this study, snow water retrievals over oceans from coincident CloudSat CPR and GPM DPR Ku-band measurements for more than 3 years are assessed. The main factors contributing to differences in snow water retrievals between CPR and DPR are carefully considered, including instrument sampling, surface precipitation phase classification, instrument sensitivity, attenuation and multiple scattering as well as surface clutter. Moreover, a set of Z_e -SWC relationships for CPR and DPR is developed using the same microphysical assumptions including snow particle-size distribution and backscattering properties of nonspherical snow particle models.

Annual mean surface snow water content distributions over oceans for one year are firstly derived from CPR and DPR reflectivities as well as the GPM 2B Combined product. It is seen that surface snow water contents from the GPM 2B Combined product are much smaller than those from DPR, possibly due to different retrieval methods. On the other hand, surface snow water contents from CPR are much larger than those from DPR at latitudes above 60° , while surface snow water contents from DPR exceed those from CPR with small differences at latitudes below 50° . Zonally mean surface snow water contents over oceans from coincident CPR and DPR measurements also display similar features. Coincident CPR and DPR snow water content profiles are further explored by dividing into two conditions. One condition is that only CPR detects the falling snow. Another condition is that both CPR and DPR detect the falling snow.

Several conclusions can be drawn from the results. First, about 88% of all snow water content profiles are under the condition that only CPR detects the falling snow. A large portion of them is associated with light snowfall events, contributing more than 20% to total surface snow water content of all CPR snow water content profiles. Second, only about 12% of all snow water content profiles are under the condition that both CPR and DPR detect the falling snow. DPR surface snow water contents are significantly larger than CPR ones in moderate and heavy snowfall events. Total surface snow water content of all DPR snow water content profiles is about 60% of total CPR surface snow water contents. Third, occurrence frequencies of surface snow water contents for DPR generally shift to larger surface snow water contents compared with those for CPR, indicating that CPR is sensitive to light snowfall events, while DPR is suitable for moderate and heavy snowfall events. Overall, mean surface water contents from CPR are much larger than those from DPR at latitudes above 60° likely due to light snowfall events misdetected by DPR, while mean surface water contents from DPR exceed those from CPR at latitudes below 50° likely due to heavy snowfall events underestimated by CPR. The discrepancy in snowfall detection capability between CPR and DPR is closely related to different instrument sensitivity, backscattering efficiency of large particles as well as attenuation and multiple scattering between CPR and DPR. In addition, it is found that DPR large minimum detectable reflectivity prevents its detection of snow water contents at high altitudes, causing a noticeable decrease in snow layer depth.

It is admitted that this study is subject to some limitations. The coincident snowfall profiles between CPR and DPR are not abundant and mainly concentrated at latitudes above 50° due to different satellite and instrument characteristics. Consequently, smaller latitudes bands (e.g., 5°) are not considered for snowfall statistical results. Since snow water content values cover a wide range from 0.001 to 1 g m^{-3} , the standard deviations of snow water contents at different latitude bands are generally large. Nevertheless, the mean value of snow water content can be related to total snow water amount at each latitude band. The surface clutter also impedes the better assessment of CPR and DPR surface snow water retrievals.

Spaceborne radars with comparable specifications at Ku- and W-bands on the same satellite are essential for global snowfall estimates. The addition of Ka-band radar can further improve global snowfall retrievals by promoting estimates of snow particle-size distributions. This configuration is realized in the upcoming ACCP mission [35,36]. ACCP architectures also carry a sub-millimeter passive microwave radiometer that can provide the

important information on cloud ice and liquid water. The results in this study are beneficial for future snowfall retrieval algorithms using spaceborne multi-sensors including multi-frequency radar and microwave radiometer.

Author Contributions: Conceptualization, M.Y.; data curation, C.Y.; formal analysis, M.Y. and C.Y.; funding acquisition, M.Y.; investigation, M.Y. and C.Y.; methodology, M.Y.; project administration, M.Y.; resources, M.Y.; software, C.Y.; supervision, M.Y.; validation, M.Y.; visualization, M.Y.; writing—original draft, M.Y. and C.Y.; writing—review and editing, M.Y. and C.Y. All authors have read and agreed to the published version of the manuscript.

Funding: This research has been supported by the National Natural Science Foundation of China (Grant No. 41905020).

Data Availability Statement: CloudSat products are available at <http://www.cloudsat.cira.colostate.edu/data-products> (accessed on 1 January 2023). GPM products are available at <https://gpm.nasa.gov/data/directory> (accessed on 1 January 2023). The CloudSat-GPM coincidence dataset is available at <https://www.cloudsat.cira.colostate.edu/community-products/cloudsat-trmm-gpm-coincidence-dataset> (accessed on 1 January 2023).

Acknowledgments: The authors thank CloudSat Data Processing Center (DPC) and National Aeronautics and Space Administration (NASA) GPM for providing standard products.

Conflicts of Interest: The authors declare no conflict of interest. The funders had no role in the design of the study; in the collection, analyses, or interpretation of data; in the writing of the manuscript, or in the decision to publish the results.

References

1. Barnett, T.P.; Dumenil, L.; Schlese, U.; Roeckner, E.; Latif, M. The effect of Eurasian snow cover on regional and global climate variations. *J. Atmos. Sci.* **1989**, *46*, 661–685. [\[CrossRef\]](#)
2. Liu, G.; Curry, J.A. Precipitation characteristics in the GIN seas determined using satellite microwave data. *J. Geophys. Res.* **1997**, *102*, 13987–13997. [\[CrossRef\]](#)
3. Viviroli, D.; Weingartner, R.; Messerli, B. Assessing the hydrological significance of the world's mountains. *Mt. Res. Dev.* **2003**, *23*, 32–40. [\[CrossRef\]](#)
4. Levizzani, V.; Laviola, S.; Cattani, E. Detection and measurement of snowfall from space. *Remote Sens.* **2011**, *3*, 145–166. [\[CrossRef\]](#)
5. Hou, A.Y.; Kakar, R.K.; Neeck, S.; Azarbarzin, A.A.; Kummerow, C.D.; Kojima, M.; Oki, R.; Nakamura, K.; Iguchi, T. The global precipitation measurement mission. *Bull. Am. Meteorol. Soc.* **2014**, *95*, 701–722. [\[CrossRef\]](#)
6. Skofronick-Jackson, G.M.; Kim, M.-J.; Weinman, J.A.; Chang, D.-E. A physical model to determine snowfall over land by microwave radiometry. *IEEE Trans. Geosci. Remote Sens.* **2004**, *42*, 1047–1058. [\[CrossRef\]](#)
7. Stephens, G.L.; Vane, D.G.; Tanelli, S.; Im, E.; Durden, S.; Rokey, M.; Reinke, D.; Partain, P.; Mace, G.G.; Austin, R.; et al. CloudSat mission: Performance and early science after the first year of operation. *J. Geophys. Res.* **2008**, *113*, D00A18. [\[CrossRef\]](#)
8. Tanelli, S.; Durden, S.L.; Im, E.; Pak, K.S.; Reinke, D.G.; Partain, P.; Haynes, J.M.; Marchand, R.T. CloudSat's cloud profiling radar after two years in orbit: Performance, calibration, and processing. *IEEE Trans. Geosci. Remote Sens.* **2008**, *46*, 3560–3573. [\[CrossRef\]](#)
9. Skofronick-Jackson, G.; Kirschbaum, D.; Petersen, W.; Huffman, G.; Kidd, C.; Stocker, E.; Kakar, R. The Global Precipitation Measurement (GPM) mission's scientific achievements and societal contributions: Reviewing four years of advanced rain and snow observations. *Q. J. R. Meteorol. Soc.* **2018**, *144* (Suppl. 1), 27–48. [\[CrossRef\]](#)
10. Draper, D.W.; Newell, D.A.; Wentz, F.J.; Krimchansky, S.; Skofronick-Jackson, G. The Global Precipitation Measurement (GPM) Microwave Imager (GMI): Instrument overview and early on-orbit performance. *IEEE J. Sel. Top. Appl. Earth Obs. Remote Sens.* **2015**, *8*, 3452–3462. [\[CrossRef\]](#)
11. Toyoshima, K.; Masunaga, H.; Furuzawa, F.A. Early evaluation of Ku- and Ka-band sensitivities for the Global Precipitation Measurement (GPM) Dual-Frequency Precipitation Radar (DPR). *Sola* **2015**, *11*, 14–17. [\[CrossRef\]](#)
12. Norin, L.; Devasthale, A.; L'Ecuyer, T.S.; Wood, N.B.; Smalley, M. Intercomparison of snowfall estimates derived from the CloudSat Cloud Profiling Radar and the groundbased weather radar network over Sweden. *Atmos. Meas. Tech.* **2015**, *8*, 5009–5021. [\[CrossRef\]](#)
13. Souverijns, N.; Gossart, A.; Lhermitte, S.; Gorodetskaya, I.V.; Grazioli, J.; Berne, A.; Duran-Alarcon, C.; Boudevillain, B.; Genthon, C.; Scarchilli, C.; et al. Evaluation of the CloudSat surface snowfall product over Antarctica using ground-based precipitation radars. *Cryosphere* **2018**, *12*, 3775–3789. [\[CrossRef\]](#)
14. Matrosov, S.Y. Comparative evaluation of snowfall retrievals from the CloudSat W-band radar using ground-based weather radars. *J. Atmos. Ocean. Technol.* **2019**, *36*, 101–111. [\[CrossRef\]](#)
15. Liu, G. Deriving snow cloud characteristics from CloudSat observations. *J. Geophys. Res.* **2008**, *113*, D00A09. [\[CrossRef\]](#)

16. Palerme, C.; Kay, J.E.; Genthon, C.; L'Ecuyer, T.; Wood, N.B.; Claud, C. How much snow falls on the Antarctic ice sheet? *Cryosphere* **2014**, *8*, 1577–1587. [[CrossRef](#)]
17. Kulie, M.S.; Milani, L.; Wood, N.B.; Tushaus, S.A.; Bennartz, R.; L'Ecuyer, T.S. A shallow cumuliform snowfall census using spaceborne radar. *J. Hydrometeor.* **2016**, *17*, 1261–1279. [[CrossRef](#)]
18. Kulie, M.S.; Milani, L. Seasonal variability of shallow cumuliform snowfall: A CloudSat perspective. *Quart. J. Roy. Meteor. Soc.* **2018**, *144* (Suppl. 1), 329–343. [[CrossRef](#)]
19. Milani, L.; Kulie, M.S.; Casella, D.; Dietrich, S.; L'Ecuyer, T.S.; Panegrossi, G.; Porcù, F.; Sanò, P.; Wood, N.B. CloudSat snowfall estimates over Antarctica and the Southern Ocean: An assessment of independent retrieval methodologies and multi-year snowfall analysis. *Atmos. Res.* **2018**, *213*, 121–135. [[CrossRef](#)]
20. Adhikari, A.; Liu, C.; Kulie, M.S. Global distribution of snow precipitation features and their properties from 3 years of GPM observations. *J. Clim.* **2018**, *31*, 3731–3754. [[CrossRef](#)]
21. Adhikari, A.; Liu, C. Geographical distribution of thundersnow events and their properties From GPMKu-band radar. *J. Geophys. Res. Atmos.* **2019**, *124*, 2031–2048. [[CrossRef](#)]
22. Chase, R.J.; Nesbitt, S.W.; McFarquhar, G.M. Evaluation of the microphysical assumptions within GPM-DPR using ground-based observations of rain and snow. *Atmosphere* **2020**, *11*, 619. [[CrossRef](#)]
23. Chase, R.J.; Nesbitt, S.W.; McFarquhar, G.M. A dual-frequency radar retrieval of two parameters of the snowfall particle size distribution using a neural network. *J. Appl. Meteor. Climatol.* **2021**, *60*, 341–359. [[CrossRef](#)]
24. Kummerow, C.D.; Randel, D.L.; Kulie, M.S.; Wang, N.-Y.; Ferraro, R.; Munchak, S.J.; Petkovic, V. The evolution of the Goddard profiling algorithm to a fully parametric scheme. *J. Atmos. Oceanic Technol.* **2015**, *32*, 2265–2280. [[CrossRef](#)]
25. Panegrossi, G.; Rysman, J.-F.; Casella, D.; Marra, A.C.; Sano, P.; Kulie, M.S. CloudSat-based assessment of GPM Microwave Imager snowfall observation capabilities. *Remote Sens.* **2017**, *9*, 1263. [[CrossRef](#)]
26. Yin, M.; Liu, G. Developing an a priori database for passive microwave snow water retrievals over ocean. *J. Geophys. Res. Atmos.* **2017**, *122*, 12960–12981. [[CrossRef](#)]
27. Rysman, J.-F.; Panegrossi, G.; Sanò, P.; Marra, A.C.; Dietrich, S.; Milani, L.; Kulie, M.S. SLALOM: An All-Surface Snow Water Path Retrieval Algorithm for the GPM Microwave Imager. *Remote Sens.* **2018**, *10*, 1278. [[CrossRef](#)]
28. Rysman, J.-F.; Panegrossi, G.; Sanò, P.; Marra, A.C.; Dietrich, S.; Milani, L.; Kulie, M.S.; Casella, D.; Camplani, A.; Claud, C.; et al. Retrieving surface snowfall with the gpm microwave imager: A new module for the slalom algorithm. *Geophys. Res. Lett.* **2019**, *46*, 13593–13601. [[CrossRef](#)]
29. Tang, G.; Wen, Y.; Gao, J.; Long, D.; Ma, Y.; Wan, W.; Hong, Y. Similarities and differences between three coexisting spaceborne radars in global rainfall and snowfall estimation. *Water Resour. Res.* **2017**, *53*, 3835–3853. [[CrossRef](#)]
30. Casella, D.; Panegrossi, G.; Sanò, P.; Marra, A.C.; Dietrich, S.; Johnson, B.T.; Kulie, M.S. Evaluation of the GPM-DPR snowfall detection capability: Comparison with CloudSat-CPR. *Atmos. Res.* **2017**, *197*, 64–75. [[CrossRef](#)]
31. Skofronick-Jackson, G.; Kulie, M.S.; Milani, L.; Munchak, S.J.; Wood, N.B.; Levizzani, V. Satellite Estimation of Falling Snow: A Global Precipitation Measurement (GPM) Core Observatory Perspective. *J. Appl. Meteor. Climatol.* **2019**, *58*, 58–1429. [[CrossRef](#)]
32. Mróz, K.; Montopoli, M.; Battaglia, A.; Panegrossi, G.; Kirstetter, P.; Baldini, L. Cross validation of active and passive microwave snowfall products over the continental United States. *J. Hydrometeor.* **2021**, *22*, 1297–1315. [[CrossRef](#)]
33. Chase, R.J.; Nesbitt, S.W.; McFarquhar, G.M.; Wood, N.B.; Heymsfield, G.M. Direct Comparisons between GPM-DPR and CloudSat Snowfall Retrievals. *J. Appl. Meteor. Climatol.* **2022**, *61*, 1257–1271. [[CrossRef](#)]
34. Turk, F.J.; Ringerud, S.E.; Camplani, A.; Casella, D.; Chase, R.J.; Ebtehaj, A.; Gong, J.; Kulie, M.; Liu, G.; Milani, L.; et al. Applications of a CloudSat-TRMM and CloudSat-GPM Satellite Coincidence Dataset. *Remote Sens.* **2021**, *13*, 2264. [[CrossRef](#)]
35. Kummerow, C.D.; Tanelli, S.; Takahashi, N.; Furukawa, K.; Klein, M.; Levizzani, V. Plans for Future Missions. In *Satellite Precipitation Measurement*; Levizzani, V., Kidd, C., Kirschbaum, D.B., Kummerow, C.D., Nakamura, K., Turk, F.J., Eds.; Springer: Cham, Switzerland, 2020; Volume 1, pp. 99–119.
36. Battaglia, A.; Kollias, P.; Dhillon, R.; Roy, R.; Tanelli, S.; Lamer, K.; Grecu, M.; Lebsock, M.; Watters, D.; Mroz, K.; et al. Spaceborne Cloud and Precipitation Radars: Status, Challenges, and Ways Forward. *Rev. Geophys.* **2020**, *58*, e2019RG000686. [[CrossRef](#)]
37. Curry, J.A.; Rossow, W.B.; Randall, D.; Schramm, J.L. Overview of Arctic cloud and radiation characteristics. *J. Clim.* **1996**, *9*, 1731–1764. [[CrossRef](#)]
38. Sims, E.M.; Liu, G. A parameterization of the probability of snow–rain transition. *J. Hydrometeor.* **2015**, *16*, 1466–1477. [[CrossRef](#)]
39. Stephens, G.L.; Wood, N.B. Properties of tropical convection observed by millimeter-wave radar systems. *Mon. Weather Rev.* **2007**, *135*, 821–842. [[CrossRef](#)]
40. Haynes, J.M.; L'Ecuyer, T.S.; Stephens, G.L.; Miller, S.D.; Mitrescu, C.; Wood, N.B.; Tanelli, S. Rainfall retrieval over the ocean with spaceborne W-band radar. *J. Geophys. Res.* **2009**, *114*, D00A22. [[CrossRef](#)]
41. Hamada, A.; Takayabu, Y.N. Improvements in Detection of Light Precipitation with the Global Precipitation Measurement Dual-Frequency Precipitation Radar (GPM DPR). *J. Atmos. Ocean. Tech.* **2016**, *33*, 653–667. [[CrossRef](#)]
42. Matrosov, S.Y.; Battaglia, A. Influence of multiple scattering on CloudSat measurements in snow: A model study. *Geophys. Res. Lett.* **2009**, *36*, L12806. [[CrossRef](#)]
43. Yin, M.; Liu, G.; Honeyager, R.; Joseph Turk, F. Observed differences of triple-frequency radar signatures between snowflakes in stratiform and convective clouds. *J. Quant. Spectrosc. Ra.* **2017**, *193*, 13–20. [[CrossRef](#)]

44. Matrosov, S.Y. Modeling backscatter properties of snowfall at millimeter wavelengths. *J. Atmos. Sci.* **2007**, *64*, 1727–1736. [[CrossRef](#)]
45. Hiley, M.J.; Kulie, M.S.; Bennartz, R. Uncertainty Analysis for CloudSat Snowfall Retrievals. *J. Appl. Meteorol. Clim.* **2011**, *50*, 399–418. [[CrossRef](#)]
46. Green, D.A. A colour scheme for the display of astronomical intensity images. *Bull. Astr. Soc. India* **2011**, *39*, 289–295.
47. Wood, N.B.; L'Ecuyer, T.S.; Heymsfield, A.J.; Stephens, G.L.; Hudak, D.R.; Rodrigues, P. Estimating snow microphysical properties using collocated multisensor observations. *J. Geophys. Res. Atmos.* **2014**, *119*, 8941–8961. [[CrossRef](#)]
48. Rodgers, C.D. Retrieval of atmospheric temperature and composition from remote measurements of thermal radiation. *Rev. Geophys.* **1976**, *14*, 609–624. [[CrossRef](#)]
49. Iguchi, T.; Seto, S.; Meneghini, R.; Yoshida, N.; Awaka, J.; Le, M.; Chandrasekar, V.; Brodzik, S.; Kubota, T.; Takahashi, N. *GPM/DPR Level-2 Algorithm Theoretical Basis Document*; NASA Goddard Space Flight Center: Greenbelt, MD, USA, 2021.
50. Olson, W.S. *The GPM Combined Radar-Radiometer Algorithm Team. GPM Combined Radar-Radiometer Precipitation Algorithm Theoretical Basis Document (Version 5)*; NASA: Washington, DC, USA, 2018.
51. Kuo, K.-S.; Olson, W.S.; Johnson, B.T.; Grecu, M.; Tian, L.; Clune, T.L.; van Aartsen, B.H.; Heymsfield, A.J.; Liao, L.; Meneghini, R. The microwave radiative properties of falling snow derived from nonspherical ice particle models. Part I: An extensive database of simulated pristine crystals and aggregate particles, and their scattering properties. *J. Appl. Meteor. and Climatol.* **2016**, *55*, 691–708. [[CrossRef](#)]
52. Liu, G. A database of microwave single-scattering properties for nonspherical ice particles. *Bull. Am. Meteorol. Soc.* **2008**, *89*, 1563. [[CrossRef](#)]
53. Honeyager, R.; Liu, G.; Nowell, H. Voronoi diagram-based spheroid model for microwave scattering of complex snow aggregates. *J. Quant. Spectrosc. Radiat. Transf.* **2016**, *170*, 28–44. [[CrossRef](#)]
54. Draine, B.T.; Flatau, P.J. Discrete-dipole approximation for scattering calculations. *J. Opt. Soc. Am. A Opt. Image Sci. Vis.* **1994**, *11*, 1491–1499. [[CrossRef](#)]
55. Braham, R.R., Jr. Snow particle size spectra in lake effect snows. *J. Appl. Meteorol.* **1990**, *29*, 200–207. [[CrossRef](#)]
56. Woods, C.P.; Stoelinga, M.T.; Locatelli, J.D. Size spectra of snow particles measured in wintertime precipitation in the Pacific Northwest. *J. Atmos. Sci.* **2008**, *65*, 189–205. [[CrossRef](#)]
57. Heymsfield, A.J.; Field, P.; Bansemer, A. Exponential size distributions for snow. *J. Atmos. Sci.* **2008**, *65*, 4017–4031. [[CrossRef](#)]

Disclaimer/Publisher's Note: The statements, opinions and data contained in all publications are solely those of the individual author(s) and contributor(s) and not of MDPI and/or the editor(s). MDPI and/or the editor(s) disclaim responsibility for any injury to people or property resulting from any ideas, methods, instructions or products referred to in the content.